Chimera Time-Crystalline Order in Quantum Spin Networks

A. Sakurai,[1,2,*] V. M. Bastidas,[3,1,†] W. J. Munro,[3,1] and Kae Nemoto[1]
[1]National Institute of Informatics, 2-1-2 Hitotsubashi, Chiyoda-ku, Tokyo 101-8430, Japan
[2]School of Multidisciplinary Sciences, Department of Informatics, SOKENDAI (The Graduate University for Advanced Studies), Shonan Village, Hayama, Kanagawa 240-0193, Japan
[3]NTT Basic Research Laboratories & Research Center for Theoretical Quantum Physics, 3-1 Morinosato-Wakamiya, Atsugi, Kanagawa 243-0198, Japan

(Received 6 July 2020; revised 11 December 2020; accepted 24 February 2021; published 26 March 2021)

Symmetries are well known to have had a profound role in our understanding of nature and are a critical design concept for the realization of advanced technologies. In fact, many symmetry-broken states associated with different phases of matter appear in a variety of quantum technology applications. Such symmetries are normally broken in spatial dimension, however, they can also be broken temporally leading to the concept of discrete time symmetries and their associated crystals. Discrete time crystals (DTCs) are a novel state of matter emerging in periodically driven quantum systems. Typically, they have been investigated assuming individual control operations with uniform rotation errors across the entire system. In this work we explore a new paradigm arising from nonuniform rotation errors, where two dramatically different phases of matter coexist in well defined regions of space. We consider a quantum spin network possessing long-range interactions where different driving operations act on different regions of that network. What results from its inherent symmetries is a system where one region is a DTC, while the second is ferromagnetic. We envision our work to open a new avenue of research on chimeralike phases of matter where two different phases coexist in space.

DOI: 10.1103/PhysRevLett.126.120606

Symmetries, while they may be a simple concept, have had a profound effect on many fields of physics and are crucial in understanding many natural phenomena [1–3] as well as the realization of many advanced technologies. This includes our well-known phases of matter (solids, liquids, and gases). Crystals as a solid with a periodic nature are one of the most familiar examples of spatial symmetry breaking [1,4–6]. One can also think of the temporal dimension and whether such symmetry breaking occurs there [7–9]. In fact, temporal symmetry breaking does occur in periodically driven nonequilibrium systems and the phase of matter that arises is referred to as discrete time crystals (DTCs) [10–30]. Recently the existence of DTCs has been demonstrated in trapped ions [31], nitrogen-vacancy spin impurities [32], nuclear spins in molecules [33], superfluid quantum gases [34], ordered dipolar many-body systems [35], and silicon doped with phosphorus [36].

In those recent demonstrations, to generate the DTC one needs to apply individual spin rotations with a uniform error across the entire system [10–14]. Of course there is no reason that one needs to utilize a uniform drive acting on the whole system. Instead the drive could be different for different regions within the system. This is particularly interesting as it means different phases of coexisting matter could be engineered. In this Letter we investigate the effect of regional driving on a system capable of supporting DTCs and explore its dynamics. We show that multiple phases of matter can coexist within the overall system. Such novel phases of matter are analogous to chimera states in classical nonlinear systems where synchronized and unsynchronized phases coexist [37–40] even in the semiclassical regime [41]. As such, we are going to consider "chimera DTCs" consisting of a DTC and an alternate phase of matter (ferromagnetic). We will generally begin with a DTC in a quantum spin network and then apply a drive to a certain region of that crystal to evolve it into the ferromagnetic phase (alternatively one could start with the ferromagnetic phase for the entire system and apply a drive to a certain region to transform that region into a DTC). This is depicted in Fig. 1(a). Both the original and the new phases of matter coexist at the same time in different regions of space (a chimeralike state) despite the spin-spin coupling throughout the network.

Let us begin with a N-spin quantum network governed by a time-periodic Hamiltonian of the form

$$\hat{H}(t)=\begin{cases}\hat{H}_1=\hbar g(1-\epsilon_A)\sum_{l\in A}\sigma_l^x+\hbar g(1-\epsilon_B)\sum_{l\in B}\sigma_l^x & 0\le t<T_1\\ \hat{H}_2=\hbar\sum_{lm}J_{lm}^z\sigma_l^z\sigma_m^z+\hbar\sum_l W_l^z\sigma_l^z & T_1\le t<T,\end{cases} \tag{1}$$

with a total period $T=T_1+T_2$ ($\hat{H}_1$ is applied for a time T_1 followed by $\hat{H}_2$ for a time T_2). The nodes of our network

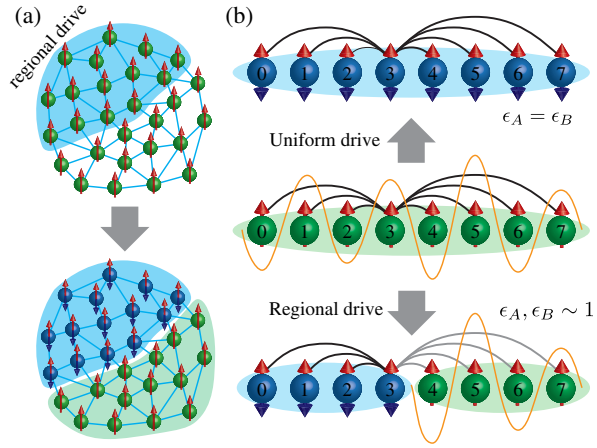

FIG. 1. Chimera discrete time crystals in a spin network. (a) Schematic illustration of the chimera time crystal in a spin network. The top panel illustrates this network under the effect of regional driving while the bottom panel shows the sublattice A (blue region), which behaves like a discrete time crystal. In contrast, the region B (green region) is in a ferromagnetic state. (b) Illustrates a $N = 8$ site spin chain where we apply regional drivings. A π rotation is applied on region A spins $l = 0, 1, 2, 3$ while small rotation is applied on the remaining spins that define region B. Here, the black and yellow lines represent the couplings J^z_{lm} between the spins and the disordered potential W_l, respectively. In the case of regional drive, the gray lines represent the weak coupling between the regions A and B.

are the individual spins at sites labeled by $l = 1, \ldots, N$. Here σ^μ_l with $\mu \in \{x, y, z\}$ are the usual Pauli operators at the lth site. Next g is a drive amplitude chosen such that $gT_1 = \pi/2$. Our Hamiltonian $\hat{H}_1$ applies separate rotations on the two well-defined spin network regions where we allow for errors ϵ_A and ϵ_B, respectively. This is shown in Fig. 1(a) as the blue region A and green region B. Further the couplings $J_{l,m}$ determine the connectivity of the network, because they can be represented by an edge joining the lth and mth nodes as depicted in Fig. 1. We also consider the effect of disorder $W^z_l \in [-W, W]$ drawn from a uniform distribution with strength W. Finally, it is worth mentioning that when $\epsilon_A = \epsilon_B \ll 1$ the whole system retains its single DTC nature [11,12].

Now let us evaluate how we can manipulate these phases of matter using regional drives. We consider the case where the rotation arising from the drive on region A is close to π (ϵ_A is small) while the drive on region B is effectively turned off (ϵ_B close to one). The local magnetization $m^z{}_l(nT) = \langle \sigma^z_l(nT) \rangle$ at the lth site measured at stroboscopic times $t_n = nT$ (with n being a natural number) can then be used to monitor the breaking of the discrete time translational symmetry and the emergence of DTC in a given region of the network.

To investigate this stroboscopic behavior, we employ the Floquet operator for a single drive period [42–45] given by

$$\hat{\mathcal{F}} = \exp\left(-\frac{i}{\hbar}\hat{H}_2 T_2\right)\exp\left(-\frac{i}{\hbar}\hat{H}_1 T_1\right). \tag{2}$$

The $2T$ periodicity of the DTC enables us to unveil the symmetries of the system at times $t_n = 2nT$. Here, the stroboscopic dynamics is generated by the square of the Floquet operator $\hat{\mathcal{F}}^2 = \exp(-2i\hat{H}^{\text{eff}}_{\epsilon_A,2T}T/\hbar)$ with $\hat{H}^{\text{eff}}_{\epsilon_A,2T}$ being the systems $2T$-effective Hamiltonian. Because of $\hat{H}^{\text{eff}}_{\epsilon_A,2T}$ structure we can use a high-frequency expansion [44,45] for the driven system to express it in the closed form $\hat{H}^{\text{eff}}_{\epsilon,2T} = \hat{H}_A + \hat{H}_B + \hat{H}_{AB}$ where

$$\begin{aligned}
\hat{H}_A &= \frac{\hbar}{2}\sum_{l,m\in A} J^z_{lm}\sigma^z_l\sigma^z_m - \frac{\hbar\pi\epsilon_A}{4}\sum_{l,m\in A} J^z_{lm}\sigma^z_l\sigma^y_m,\\
\hat{H}_B &= \frac{\hbar}{2}\sum_{l,m\in B} J^z_{lm}\sigma^z_l\sigma^z_m + \frac{\hbar}{2}\sum_{l\in B} W_l\sigma^z_l,\\
\hat{H}_{AB} &= -\frac{\hbar\pi\epsilon_A}{4T}\sum_{l\in A}[(\cos\hat{\theta}_l + 1)\sigma^x_l + \sin\hat{\theta}_l\sigma^y_l].
\end{aligned} \tag{3}$$

Here we have assumed for convenience $\epsilon_A \ll 1$ and $\epsilon_B = 1$ (this simplification will be relaxed in our simulations).

The coupling Hamiltonian $\hat{H}_{AB}$ is strongly dependent on the operator $\hat{\theta}_l = 2W_lT_2 + 2T_2\sum_{m\in B} J^z_{lm}\sigma^z_m$ for the lth sites in A [46]. Setting $\epsilon_A = 0$, the regions A and B are decoupled at times $t_n = 2nT$. This indicates that each region preserves the local operators σ^z_l and its own symmetries. Region A holds a $\mathbb{Z}_2$-Ising symmetry $\sigma^z_l = -\sigma^z_l$ which may be broken in B due to the disorder. Remarkably for $\epsilon_A \ll 1$, $\hat{H}^{\text{eff}}_{\epsilon_A,2T}$ breaks the $U(1)$ symmetry in region A while $\hat{H}_B$ associated with region B remains conserved with $[\hat{H}_B, \hat{H}^{\text{eff}}_{\epsilon_A,2T}] = [\sigma^z_l, \hat{H}^{\text{eff}}_{\epsilon_A,2T}] = 0$. This creates the *chimera* DTC where two phases of matter emerges in a network of spins.

To explore the dynamics (the emergence) of chimera DTCs we consider a particular example of a one-dimensional array of $N = 8$ spins. Here the coupling strength between spins is dependent on the distance they are apart with coupling strength $J^z_{lm} \equiv J_0/|l - m|^\alpha$ for the sites l and m. While the geometrical arrangement of spin is one dimensional, the parameter α determines the structure of the network. For example, if $\alpha = 0$ the network is all-to-all connected and for $\alpha = \infty$, it has nearest-neighbor coupling only. It is important to note that our results are general and can be applied to other networks with more complex connectivities (see Supplemental Material [46]). Choosing an initial state $|\Psi(0)\rangle_z = |1, 1, \ldots, 1\rangle_z$ which breaks the $\mathbb{Z}_2$-Ising symmetry, we can now explore, as illustrated in Fig. 1(b), the effect of $\epsilon_A \ll 1$ and $\epsilon_B \sim 1$ on the system's magnetization. Here we set $T_1 = T_2 = T/2$ and determine the magnetization at $t_n = 2nT$. Its dynamics is characterized by the ratio $\delta_x = \epsilon_A\pi(1 + \overline{\langle\cos(\hat{\theta})\rangle})/2J_0T$, where $\overline{\langle\cdots\rangle}$ is the ensemble average. This indicates the balance between the

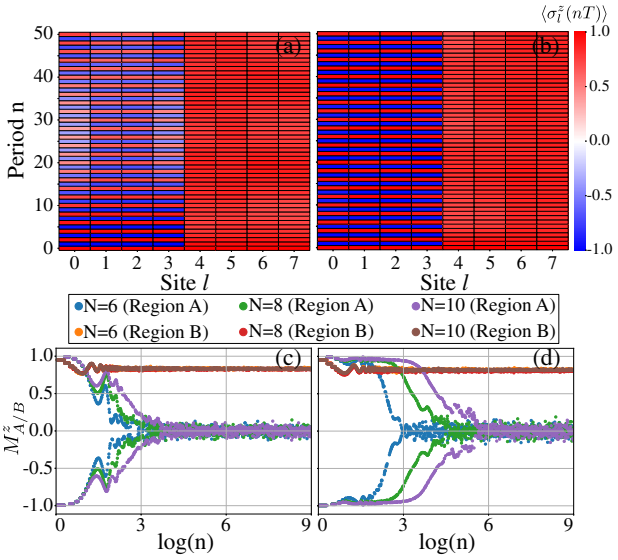

FIG. 2. The short-time dynamics of the local magnetization $\langle\sigma_l^z(t)\rangle$ for a chimera DTC in the weak $J_0T = 0.072$ (a) and strong $J_0T = 0.2$ (b) coupling regimes, respectively. Here, we have chosen $\epsilon_A = 0.03$, $\epsilon_B = 0.9$, $gT = \pi$, $\alpha = 1.51$, and $WT = 2\pi$ with an initial state $|\Psi(0)\rangle_z = |1, 1, \ldots, 1\rangle$. Next the long-time dynamics of the regional magnetization $M^z_{A/B} = 2/N\sum_{l\in A/B}\langle\sigma_l^z(t)\rangle$ are shown for weak (c) and strong (d) couplings and different system sizes $N = 6$, 8, 10.

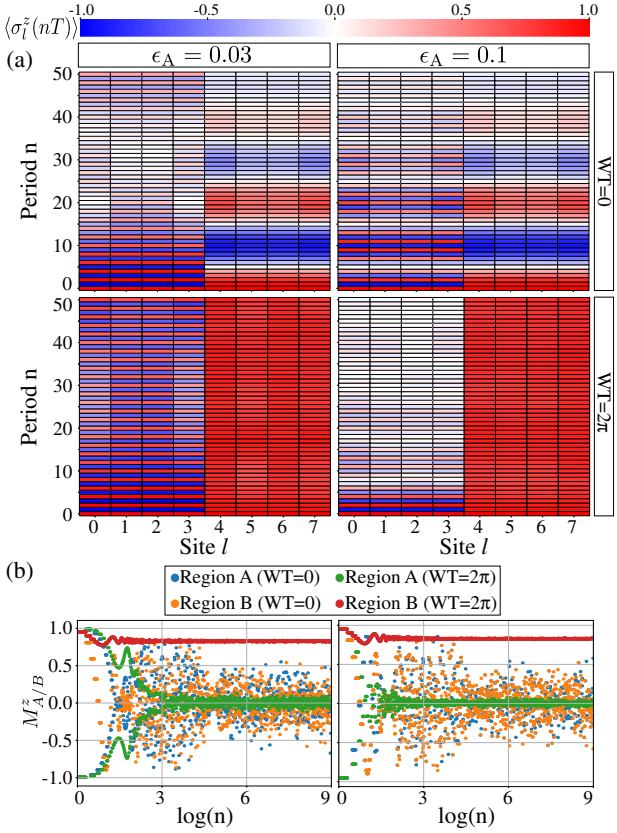

FIG. 3. The stroboscopic evolution (a) of the ensemble averaged local magnetization $\langle\sigma_l^z(nT)\rangle$ over 100 realizations of disorder for a chimera DTC in the weak coupling regime over short times. Here two specific values of ϵ_A are chosen ($\epsilon_A = 0.03, 0.1$) with disorder strengths $WT = 0, 2\pi$. The other parameters are the same as in Fig. 2 including $|\Psi(0)_z\rangle = |1, 1, \ldots, 1\rangle$ as our initial state. In (b) we show the long-time dynamics of the regional magnetization $M^z_{A/B}$ for errors $\epsilon_A = 0.03, 0.1$ (left, right panels), respectively. Here, the blue and green curves represent the regional magnetization M^z_A of region A for disorder strengths $WT = 0, 2\pi$ respectively, while the orange and red curves represent the regional magnetization M^z_B in region B for $WT = 0, 2\pi$. The regional magnetization M^z_A is periodic with period $2T$, whereas M^z_B is constant under the effect of disorder. This leads to the coexistence in space of the DTC and ferromagnetic phase.

effective transverse magnetic field felt by A due to the coupling $\hat{H}_{AB}$, and the interaction strength J_0. It has a critical point at $\delta_x^c \sim 1$. We employ two different values of $\epsilon_A = 0.1$, 0.03 to investigate the dynamics above and below that critical point. The second term in $\hat{H}^{\text{eff}}_{\epsilon_A,2T}$ can be neglected as $J_0\epsilon_A \ll 1$, however we need to consider disorder as another factor in the DTCs emergence (disorder is essential for the DTC to be stabilized under the imperfect rotations [12]). The short-time magnetization dynamics clearly shows two different behaviors in regions A and B as shown in Figs. 2(a) and 2(b) for the weak $(J_0T = 0.072)$, strong $(J_0T = 0.2)$ couplings respectively. In region A, the regional rotation breaks the discrete time translational symmetry yielding the DTC phase, while region B retains its ferromagnetic phase. It is also important to explore the long-time dynamics for different system sizes in the weak and strong coupling regimes which we show in Figs. 2(c) and 2(d). It is clearly seen in this long-time regime that the DTCs melt [48–50]. Two coexistent phases of matter are still present.

It is important to explore the effect of rotation errors and disorder on our chimera DTC. Such effects are more prominent in the weak coupling regime. In Fig. 3 we plot the magnetization's dynamics for different values of ϵ_A and disorder strengths W_l. These are chosen randomly in the interval $[0, W]$, where $WT = 0$ correspond to the no disorder case, while $WT = 2\pi$ is strong disorder. We employ 100 realizations in determining our ensemble average. In the regime $\delta_x < 1$ $(\epsilon_A = 0.03)$ our chimera DTC emerges. Increasing W stabilized the DTC in region A. This is not unexpected as $\hat{H}^{\text{eff}}_{\epsilon_A,2T}$ can be seen as the Ising model perturbed by an effective transverse magnetic field $\hat{H}_{AB}$. The weaker the effective magnetic field (larger W), the more stable the DTC is.

In more detail, in the absence of disorder $WT = 0$, region A feels a uniform transverse field with strength $\hbar\pi\epsilon_A/2T$ and the value $\delta_x = \epsilon_A\pi/J_0T$ for $\epsilon_A = 0.03$ is effectively close to the critical point. Because of the effect of the transverse magnetic field, the paramagnetic phase wins over the DTC phase as the time goes on, and the chimera DTC transforms into a new chimera phase of paramagnetic

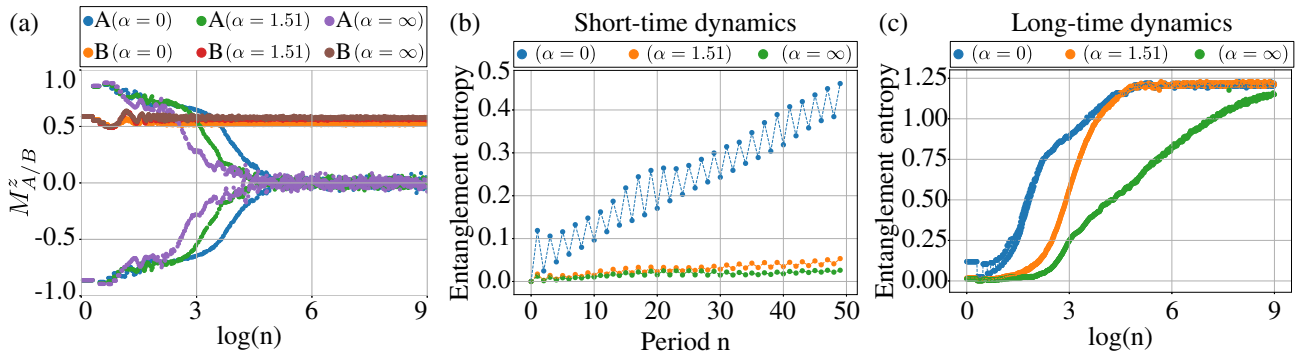

FIG. 4. In (a) we plot the ensemble average of the regional magnetizations $M^z_{A/B}$ versus stroboscopic time for $\alpha = 0, 1.51, \infty$. We have used our typical strong coupling regime parameters: $J_0T = 0.2, \epsilon_A = 0.03, \epsilon_B = 0.9$, $gT = \pi$, and with disorder strength $WT = 2\pi$. Next (b),(c) illustrate the short- and long-time entanglement $S_B(nT)$ dynamics. Our ensemble averaging utilizes 100 realizations of the disorder with the initial state $|\Psi(0)\rangle_{z,\theta} = e^{-i\sum_l (\theta/2)\sigma^x_l}|\Psi(0)\rangle_z$ where $\theta = 0.2\pi$.

and ferromagnetic phases. With disorder $\overline{\langle\cos(\hat{\theta})\rangle} \approx \overline{\langle\sin(\hat{\theta})\rangle} \approx 0$ meaning the magnetic field is effectively suppressed. In this case, $\delta_x = \epsilon_A\pi/2J_0T$ remains effectively small and the DTC phase of region A becomes stable. These effects are shown in see Fig. 3(a). When $\delta_x > 1$ ($\epsilon_A = 0.1$) the transverse magnetic field is dominant in the effective Hamiltonian $\hat{H}^{\text{eff}}_{\epsilon,2T}$ meaning the system exhibits many-body Rabi oscillations. In the absence of disorder, the local magnetization at each site of the region A oscillates with the same frequency. On the contrary, the disorder randomizes the frequencies of the Rabi oscillations smoothing it out when the ensemble average is taken. Such behavior is illustrated in Figs. 3(a) and 3(b) for the short- and long-time dynamics in the weak coupling regime. As it is shown in Fig. 3(a), in the absence of disorder the spins in region B also oscillate with the same frequency. This means that the disorder stabilizes the magnetizations in region B at stroboscopic times.

The above analysis has shown that the chimera phase can be observed from the magnetization dynamics of our quantum system and is stable for $\delta_x < 1$. It is useful at this stage to focus our attention in the strong coupling regime (less sensitive to rotational errors) to explore the effect of long-range correlations and how they affect the observed macroscopic behavior. The archetypical quantum behavior is of course entanglement. Given our system remains pure state throughout its evolution, we can evaluate the degree of entanglement [51,52] between the two regions A and B using the von Neumann entropy $S_B(t) = -\text{Tr}_B[\hat{\rho}_B(t)\ln\hat{\rho}_B(t)]$ where $\hat{\rho}_B(t) = \text{Tr}_A[|\Psi(t)\rangle\langle\Psi(t)|]$ is the reduced density matrix of region B (other entanglement measures could be used if desired). In our exploration of entanglement in this chimera DTC we need to consider both the effect of rotation errors $\epsilon_{A,B}$ and errors in the initial state preparation. For the later case we will simply model our initial state as $|\Psi(0)\rangle_{z,\theta} = e^{-i\sum_l (\theta/2)\sigma^x_l}|\Psi(0)\rangle_z$, where θ is the error. As $|\Psi(0)\rangle_{z,\theta\neq 0}$ are not eigenstates of $\hat{H}(t)$ we expect interesting dynamics to arise. In Fig. 4(a) we plot the regional magnetization $M^z_{A/B}$ versus time for various α (interaction range) by considering $\epsilon_A = 0.03$, $\epsilon_B = 0.9$, and $\theta = 0.2\pi$ with disorder strength $WT = 2\pi$. We compare the magnetization dynamics for three different α's ($\alpha = 0, 1.51, \infty$) where $\alpha = 1.51$ was chosen based on the recent experiments [31]. The $\alpha = 0$ and $\alpha = \infty$ values correspond to all-to-all coupling and nearest-neighbor coupling respectively. Figure 4(a) shows that the chimera DTC is robust against errors and two phases of matter (DTC and ferromagnetic) coexist for a long time that depends on the interaction range α. This shows that the chimera DTC is more stable for all-to-all coupling ($\alpha = 0$) where it has the longest lifetime.

So far we have shown that the chimera DTC is robust against errors in both rotations and state preparation. The natural question that arises is how the degree of entanglement between regions A and B varies with long-range connectivity and the effect of rotation errors on it. In Figs. 4(b) and 4(c) we plot the short- and long-time entanglement dynamics for three α values. For times where the DTC is stable [see Fig. 4(b)] the degree of entanglement is small for short-range interactions ($\alpha = 1.51, \infty$) but increases as more long-range interactions are included ($\alpha = 0$). In the long-time limit, the DTC in region A melts and the entanglement reaches a steady state value that depends on the interaction range α. The reason are local conserved quantities within the DTC phase that prevent long-range correlations between regions A and B. When the DTC in region A melts, quantum tunneling is possible between the different localized states resulting in an increase in entanglement between regions A and B. This is shown in Fig. 4(c). Here it is important to compare our results with the entanglement entropy for generic thermal and many-body localized (MBL) states. If the system is thermalized, the average entanglement entropy is predicted to be $\overline{\langle S\rangle} \sim [N\ln(2) - 1]/2 \approx 2.3$ for $N = 8$. On the contrary, in the MBL phase the predicted average entropy

should be $\overline{\langle S\rangle} \sim \ln(2) \approx 0.69$. In our chimera DTC, the interaction range α controls the degree of the correlations between regions A and B. For all the α's, the entanglement entropy eventually converges to an intermediate value $\overline{\langle S\rangle} \sim 1.23$. This means that even when the DTC in region A is melted, the entanglement entropy of our system lies between the values of a fully thermal and MBL states.

In summary, we have shown how regional driving on quantum spin networks can manipulate the phases of matter associated with it. In particular we have demonstrated how chimera DTCs can emerge using that regional driving and are stable to imperfections. Of course, we are not restricted to two regions and can apply drives in multiple regions to generate even more complex chimeralike phases. We could, for instance, create chimera phases composed of distinct DTCs surrounded by ferromagnetic or even ergodic domains. The separability of these distinct phase regions is not required for the chimera DTCs to appear. Entanglement can be present at the stroboscopic times $2nT$. It is also interesting that in the chimera DTCs the amount of entanglement is rather suppressed despite the broad interactions across the spin network. This suggests that the chimera DTCs may be used to control subsystems of a spin network. Our results are experimentally realizable with the quantum technologies available today in various platforms including superconducting circuits, trapped ions, and cold atoms.

We thank M. P. Estarellas, and T. Osada for valuable discussions. V. M. B. acknowledges fruitful discussions with E. Schöll. This work was supported in part from the Japanese MEXT Quantum Leap Flagship Program (MEXT Q-LEAP) Grant No. JPMXS0118069605, the MEXT KAKENHI Grant-in-Aid for Scientific Research on Innovative Areas Science of hybrid quantum systems Grant No. 15H05870 and the JSPS KAKENHI Grant No. 19H00662.

*akitada-phy@nii.ac.jp
†victor.m.bastidas.v.yr@hco.ntt.co.jp

[1] L. D. Landau and E. M. Lifschitz, *Course of Theoretical Physics* (Pergamon Press, New York, 1981), Vol. 9, Pt. 2.
[2] C. N. Yang and R. L. Mills, Phys. Rev. **96**, 191 (1954).
[3] J. P. Lowe and K. Peterson, *Quantum Chemistry* (Elsevier, New York, 2011).
[4] L. N. Cooper, Phys. Rev. **104**, 1189 (1956).
[5] S. L. Sondhi, S. M. Girvin, J. P. Carini, and D. Shahar, Rev. Mod. Phys. **69**, 315 (1997).
[6] P. W. Higgs, Phys. Rev. Lett. **13**, 508 (1964).
[7] F. Wilczek, Phys. Rev. Lett. **109**, 160401 (2012).
[8] P. Bruno, Phys. Rev. Lett. **111**, 070402 (2013).
[9] H. Watanabe and M. Oshikawa, Phys. Rev. Lett. **114**, 251603 (2015).
[10] K. Sacha, Phys. Rev. A **91**, 033617 (2015).
[11] K. Sacha and J. Zakrzewski, Rep. Prog. Phys. **81**, 016401 (2018).
[12] D. V. Else, C. Monroe, C. Nayak, and N. Y. Yao, Annu. Rev. Condens. Matter Phys. **11**, 467 (2020).
[13] D. V. Else, B. Bauer, and C. Nayak, Phys. Rev. Lett. **117**, 090402 (2016).
[14] V. Khemani, A. Lazarides, R. Moessner, and S. L. Sondhi, Phys. Rev. Lett. **116**, 250401 (2016).
[15] W. Berdanier, M. Kolodrubetz, S. Parameswaran, and R. Vasseur, Proc. Natl. Acad. Sci. U.S.A. **115**, 9491 (2018).
[16] K. Giergiel, A. Miroszewski, and K. Sacha, Phys. Rev. Lett. **120**, 140401 (2018).
[17] L. Guo and P. Liang, New J. Phys. **22**, 075003 (2020).
[18] L. Guo, M. Marthaler, and G. Schön, Phys. Rev. Lett. **111**, 205303 (2013).
[19] L. Guo and M. Marthaler, New J. Phys. **18**, 023006 (2016).
[20] A. Russomanno, F. Iemini, M. Dalmonte, and R. Fazio, Phys. Rev. B **95**, 214307 (2017).
[21] A. Pizzi, J. Knolle, and A. Nunnenkamp, arXiv: 1910.07539.
[22] A. Pizzi, J. Knolle, and A. Nunnenkamp, Phys. Rev. Lett. **123**, 150601 (2019).
[23] F. M. Surace, A. Russomanno, M. Dalmonte, A. Silva, R. Fazio, and F. Iemini, Phys. Rev. B **99**, 104303 (2019).
[24] F. Lemini, A. Russomanno, J. Keeling, M. Schirò, M. Dalmonte, and R. Fazio, Phys. Rev. Lett. **121**, 035301 (2018).
[25] F. M. Gambetta, F. Carollo, M. Marcuzzi, J. P. Garrahan, and I. Lesanovsky, Phys. Rev. Lett. **122**, 015701 (2019).
[26] A. Riera-Campeny, M. Moreno-Cardoner, and A. Sanpera, Quantum **4**, 270 (2020).
[27] M. P. Estarellas, T. Osada, V. M. Bastidas, B. Renoust, K. Sanaka, W. J. Munro, and K. Nemoto, Sci. Adv. **6**, eaay8892 (2020).
[28] V. M. Bastidas, M. P. Estarellas, T. Osada, K. Nemoto, and W. J. Munro, Phys. Rev. B **102**, 224307 (2020).
[29] W. C. Yu, J. Tangpanitanon, A. W. Glaetzle, D. Jaksch, and D. G. Angelakis, Phys. Rev. A **99**, 033618 (2019).
[30] V. K. Kozin and O. Kyriienko, Phys. Rev. Lett. **123**, 210602 (2019).
[31] J. Zhang, P. W. Hess, A. Kyprianidis, P. Becker, A. Lee, J. Smith, G. Pagano, I.-D. Potirniche, A. C. Potter, A. Vishwanath, N. Y. Yao, and C. Monroe, Nature (London) **543**, 217 (2017).
[32] S. Choi, J. Choi, R. Landig, G. Kucsko, H. Zhou, J. Isoya, F. Jelezko, S. Onoda, H. Sumiya, V. Khemani, C. von Keyserlingk, N. Y. Yao, E. Demler, and M. D. Lukin, Nature (London) **543**, 221 (2017).
[33] S. Pal, N. Nishad, T. S. Mahesh, and G. J. Sreejith, Phys. Rev. Lett. **120**, 180602 (2018).
[34] J. Smits, L. Liao, H. T. C. Stoof, and P. van der Straten, Phys. Rev. Lett. **121**, 185301 (2018).
[35] J. Rovny, R. L. Blum, and S. E. Barrett, Phys. Rev. Lett. **120**, 180603 (2018).
[36] J. O'Sullivan, O. Lunt, C. W. Zollitsch, M. Thewalt, J. J. Morton, and A. Pal, arXiv:1807.09884.
[37] Y. Kuramoto and D. Battogtokh, Nonlinear Phenom. Complex Syst. **5**, 380 (2002), http://www.j-npcs.org/abstracts/vol2002/v5no4/v5no4p380.html.

[38] D. M. Abrams and S. H. Strogatz, Phys. Rev. Lett. **93**, 174102 (2004).
[39] M. J. Panaggio and D. M. Abrams, Nonlinearity **28**, R67 (2015).
[40] A. M. Hagerstrom, T. E. Murphy, R. Roy, P. Hövel, I. Omelchenko, and E. Schöll, Nat. Phys. **8**, 658 (2012).
[41] V. M. Bastidas, I. Omelchenko, A. Zakharova, E. Schöll, and T. Brandes, Phys. Rev. E **92**, 062924 (2015).
[42] G. Floquet, Ann. Sci. Ecol. Norm. Sup. **12**, 47 (1883).
[43] M. Grifoni and P. Hänggi, Phys. Rep. **304**, 229 (1998).
[44] M. Bukov, L. D'Alessio, and A. Polkovnikov, Adv. Phys. **64**, 139 (2015).
[45] S. Restrepo, J. Cerrillo, V. M. Bastidas, D. G. Angelakis, and T. Brandes, Phys. Rev. Lett. **117**, 250401 (2016).
[46] See Supplemental Material at http://link.aps.org/supplemental/10.1103/PhysRevLett.126.120606 for a detailed derivation of the $2T$-effective Hamiltonian and additional numerical results, which includes Ref. [44].
[47] R. Scharf, J. Phys. A **21**, 2007 (1988).
[48] F. Machado, D. V. Else, G. D. Kahanamoku-Meyer, C. Nayak, and N. Y. Yao, Phys. Rev. X **10**, 011043 (2020).
[49] T.-S. Zeng and D. N. Sheng, Phys. Rev. B **96**, 094202 (2017).
[50] D. V. Else, B. Bauer, and C. Nayak, Phys. Rev. X **7**, 011026 (2017).
[51] R. Horodecki, P. Horodecki, M. Horodecki, and K. Horodecki, Rev. Mod. Phys. **81**, 865 (2009).
[52] J. Eisert, M. Cramer, and M. B. Plenio, Rev. Mod. Phys. **82**, 277 (2010).